Quantum tunnelling of magnetization in the single-molecule magnet Mn_6

Stefan Bahr,[a] Constantinos J. Milios,[b] Leigh F. Jones,[b] Euan K. Brechin,[b] Vincent Mosser[c] and Wolfgang Wernsdorfer*[a]

Received (in Montpellier, France) 11th December 2008, Accepted 25th February 2009
First published as an Advance Article on the web 7th April 2009
DOI: 10.1039/b822305j

We present magnetization measurements of the single-molecule magnet Mn_6 revealing various tunnel transitions inconsistent with a giant spin description. We propose a dimeric model of the molecule with two coupled spins $S = 6$, which involves crystal field anisotropy, symmetric Heisenberg exchange interaction and an antisymmetric Dzyaloshinskii–Moriya exchange interaction. We show that this simplified model of the molecule explains the experimentally observed tunnel transitions and that the antisymmetric exchange interaction between the spins gives rise to tunnelling processes between spin states belonging to different spin multiplets.

Introduction

Single-molecule magnets (SMMs)[1] have been studied intensively in recent years because their unique features allow the crossover between classical and quantum physics to be observed.[2] The macroscopic observation of quantum phenomena such as tunnelling between different spin states[3,4] or quantum interference between tunnelling paths[5,6] provides the possibility of studying in detail quantum mechanical laws in nano-scale molecular systems and also might provide substantial information concerning the implementation of spin-based solid state qubits[7–9] and molecular spintronics.[10]

During the last ten years the spin system of SMMs has mainly been described by a single macroscopic spin and the associated tunnelling processes were transitions inside a multiplet with total spin S, *i.e.* transitions which conserve the total spin S of the molecule.[2–6,11] Recent developments in the field of molecular magnetism go beyond this giant spin approximation.[12–18]

When describing the molecule as an object composed of several exchanged coupled spins s_i the total spin S of the molecule is not fixed, but several multiplets with different total spin S appear and as a consequence the allowed tunnel transitions and relaxation paths of the spin system increase considerably. The associated tunnel processes between different spin states in this multi-spin description do not need to conserve the total spin S of the molecule. Recently Carretta *et al.* showed evidence of this quantum superposition of spin states with different total spin length in the SMM Cr_7Ni by inelastic neutron scattering (INS) techniques.[13] In fact, when introducing an antisymmetric exchange coupling (Dzyaloshinskii–Moriya interaction) between the spins s_i which compose the molecule, the superposition of a symmetric and an antisymmetric spin state becomes possible. The associated tunnelling process and also quantum interference effects of different tunnelling paths have been observed recently in a Mn_{12}-based molecular wheel.[15,16,18]

In this article we report the observation of quantum tunnelling between spin states with different total spin S in a Mn-based SMM[17] currently having the highest anisotropy barrier of 89 K.[19] A theoretical model is proposed that describes the molecule as an exchange-coupled system of two separated spins $S_i = 6$. The experimentally obtained tunnel splittings using the Landau–Zener method of various symmetric and antisymmetric tunnel transitions are compared to this theoretical model.

Experimental techniques

The measurements are performed using a superconducting vector magnet and a dilution cryostat at low temperatures in the range of 100 mK to 1 K. The magnetization of the Mn_6 sample is measured by a Hall magnetometer.[20,21] The Hall bars were patterned using photolithography and dry etching, in a delta-doped AlGaAs–InGaAs–GaAs pseudomorphic heterostructure using molecular beam epitaxy (MBE). A two-dimensional electron gas is induced in the 13 nm thick $In_{0.15}Ga_{0.85}As$ well by the inclusion of a Si delta-doping layer in the graded $Al_xGa_{1-x}As$ barrier. All layers, apart from the quantum well, are fully depleted of electrons and holes. The two-dimensional electron gas density n_s is about 8.9×10^{11} cm^{-2} in the quantum well, corresponding to a sensitivity of about 700 Ω T^{-1}, essentially constant under -100 °C. The micrometre-sized sample is placed on top of the 10 μm × 10 μm Hall junction, with its easy axis approximately parallel to the magnetic field along the z-direction of the solenoid using the transverse field method.[22] The SMM has the chemical formula $[Mn^{III}_6O_2(Et\text{-}sao)_6(O_2CPh(Me)_2)_2(EtOH)_6]$ ($Et\text{-}saoH_2$ = 2-hydroxyphenylpropanone oxime) (Fig. 1a) and will be called briefly Mn_6. The structural details of the molecule and preparation of the molecule are described elsewhere.[19] The six Mn atoms, each having a spin $s_i = 2$, form the core of the molecule and they are strongly super-exchange coupled and act as a macroscopic spin $S = 12$ at low temperature.[19]

[a] *Institut Néel, CNRS & Université J. Fourier, BP 166, 38042, Grenoble Cedex 9, France. E-mail: wolfgang.wernsdorfer@grenoble.cnrs.fr*
[b] *School of Chemistry, The University of Edinburgh, West Mains Road, Edinburgh, UK EH9 3JJ*
[c] *Itron France, 76 avenue Pierre Brossolette, 92240, Malakoff, France*

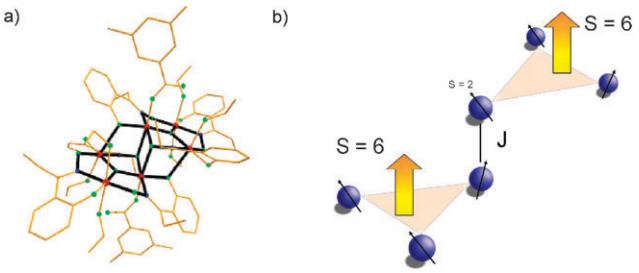

Fig. 1 (a) Structure of the molecule Mn_6, where the core of the molecule is highlighted (manganese (red), oxygen (green), nitrogen (blue)).[19] (b) Simplified model of the magnetic core of the Mn_6 molecule with two ferromagnetically coupled spin triangles, each containing three manganese atoms and having a total spin $S = 6$, which form the dimeric molecule.

Results and discussion

General discussion of the spin system

The recent work of Carretta *et al.* employing INS techniques shows evidence of very low-lying excited spin multiplets in Mn_6 and as a result shows the breakdown of the giant spin model.[14] In contrast to Carretta *et al.* we propose to describe the molecule by two superexchange coupled spin triangles, each of them being described by a rigid total spin $S = 6$ (see Fig. 1b).[17] This simplified molecular dimer description is in very good agreement with the INS measurements and simulations shown by Carretta *et al.* Our model reproduces very well the low-lying spin multiplets and gives the advantage of a quite small Hilbert and parameter space compared to the description of the Mn_6 molecule by Carretta *et al.*[14]

Each of the two ferromagnetically coupled spins of the molecular dimer $S_1 = S_2 = 6$ can be described by the spin Hamiltonian:

$$\mathscr{H}_i = -D(S_i^z)^2 - g\mu_B\mu_0 \boldsymbol{S}_i\boldsymbol{H} \qquad (1)$$

where S_i^x, S_i^y and S_i^z are the vector components of the i-th spin operator, $g = 1.99$ is the gyromagnetic factor and μ_B is the Bohr magneton. The first term describes the uniaxial anisotropy of the molecule with longitudinal anisotropy parameter D and the second term is the Zeeman interaction of the spin $\boldsymbol{S}_i$ with an external magnetic field $\boldsymbol{H}$.

The exchange interaction of the two halves of the molecule—as depicted in Fig. 1b—can be described by

$$\mathscr{H}_{ex} = -J\boldsymbol{S}_1\,\boldsymbol{S}_2 + \boldsymbol{D}_{12}\,(\boldsymbol{S}_1 \times \boldsymbol{S}_2) \qquad (2)$$

where the first term describes the isotropic Heisenberg exchange interaction with exchange constant J and the second term is an antisymmetric Dzyaloshinskii–Moriya (DM) interaction between the two spins. These antisymmetric interactions result in general from pairwise interactions of neighbouring spins that do not have an inversion centre. This condition is fulfilled in the Mn_6 molecule even when the entire molecule has an inversion centre. It is extremely unlikely that all these individual DM contributions would cancel out for all applied fields, and all possible excitations and dynamics. The possibility of a DM interaction in the Mn_6 molecule is thus well justified.

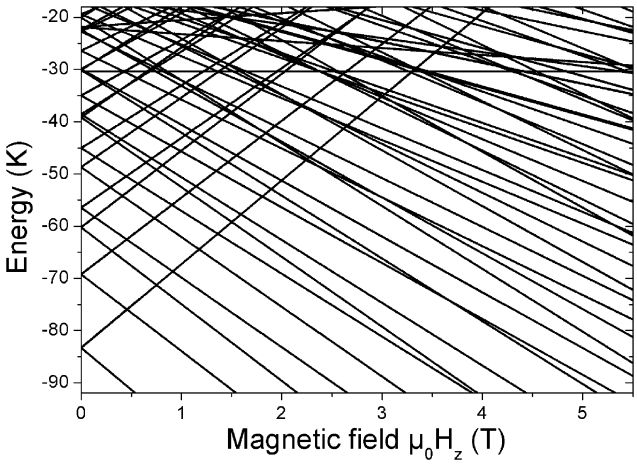

Fig. 2 Zeeman diagram of the dimeric molecule Mn_6 using the longitudinal anisotropy constant $D = 1.28$ K, an isotropic Heisenberg exchange interaction $J = 0.8$ K and $g = 1.99$. Due to the exchange interaction some excited spin multiplets are located only a few Kelvin above the ground state.

Exact diagonalization of the total spin Hamiltonian $\mathscr{H} = \mathscr{H}_1 + \mathscr{H}_2 + \mathscr{H}_{ex}$ leads to the energy spectrum shown in Fig. 2. The lowest lying spin states belong to the $S = 12$ multiplet. Due to the ferromagnetic exchange the first excited spin multiplet $|S = 11, M_S = \pm 11\rangle$ is located at about 25 K above the ground state doublet $|S = 12, M_S = \pm 12\rangle$ in zero magnetic field. In the following we will discuss the different level crossings not in the eigenbasis of the total spin of the molecule $|S, M_S\rangle$. As the total spin of the molecule may fluctuate we chose the more convenient eigenbasis of the two single spins of the molecule $|S_1,m_1\rangle \otimes |S_2,m_2\rangle \equiv |m_1,m_2\rangle$. The ground state doublet can be expressed as $|12, \pm 12\rangle \equiv |\pm 6, \pm 6\rangle$ and the first doublet of the first excited multiplet reads $|11, \pm 11\rangle \equiv 1/\sqrt{2}(|\pm 6, \pm 5\rangle - |\pm 5, \pm 6\rangle)$. The lowest lying spin eigenstates belonging to the ground state multiplet $S = 12$ are symmetric in respect to a permutation of the two spins in the product base $|m_1\rangle \otimes |m_2\rangle$, whereas the eigenstates of the $S = 11$ multiplet are antisymmetric in this single spin eigenbasis.

When we look at the probability of tunnelling from one spin state to another, we see immediately that most of the terms in the Hamiltonian $\mathscr{H}$ are symmetric and therefore only provide coupling between symmetric spin states. The only antisymmetric term in the Hamiltonian is the DM exchange interaction, and as a consequence this term can provide a coupling between a symmetric and an antisymmetric spin state, *i.e.* this term couples spin states of the ground state multiplet $S = 12$ and the first excited multiplet $S = 11$.

Tunnel transitions at low longitudinal magnetic field

Fig. 3 shows some magnetization measurements at low temperature in the presence of large transverse magnetic fields at different sweep rates. Equally spaced and very pronounced steps of the magnetization appear at approximately $\mu_0 H_z \approx 0$ T, 0.45 T, 0.9 T, 1.35 T and 1.8 T. In between these tunnel transitions, we observe a fine structure of smaller steps, which occur at approximately $\mu_0 H_z \approx 1.2$ T and 1.65 T.

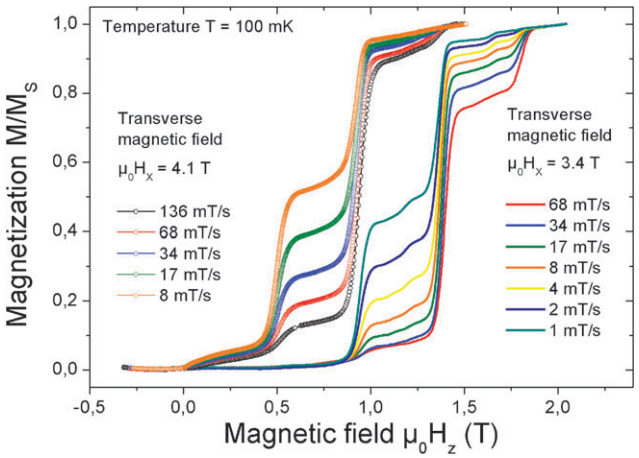

Fig. 3 Magnetization measurements of Mn_6 for different field sweep rates and two transverse magnetic fields $\mu_0H_x = 3.4$ T (solid lines) and $\mu_0H_x = 4.1$ T (open symbols). The sample was first saturated in a large negative magnetic field and then ramped at constant sweep rate to positive field. All measurements were done at low temperature $T = 100$ mK.

Fig. 4 shows the derivatives of the magnetization curves of Fig. 3 as well as the corresponding Zeeman diagram with the lowest energy levels. The main steps of magnetization, equally spaced by $\Delta\mu_0H_z \approx 0.45$ T, can be explained in the framework of a giant spin approximation, when describing the molecule by a collective spin $S = 12$. We checked that the fine structure is not due to spin–spin cross-relaxation.[23] Additionally, the fine structure cannot be explained when assuming small differences in the crystal field parameters in the two halves of the molecule.

However, the fine structure in the magnetization steps is related to excited spin multiplets. In fact, these steps can be understood when considering excited spin multiplets in the multi-spin approach. For example the tunnel transition at $\mu_0H_z \approx 0.45$ T involves the symmetric eigenstates $|-6, -6\rangle$ and $1/\sqrt{2}(|6, 5\rangle + |5, 6\rangle)$. In between the main, equally spaced tunnel transitions several avoided level crossings appear that involve excited spin multiplets (as shown in Fig. 4).

As an example, the avoided level crossing at $\mu_0H_z \approx 0.75$ T involves the symmetric eigenstate $|-6, -6\rangle$ and the antisymmetric eigenstate $1/\sqrt{2}(|6, 5\rangle - |5, 6\rangle)$. The tunnel process at $\mu_0H_z \approx 1.2$ T involves the symmetric eigenstate $|-6, -6\rangle$ and the antisymmetric eigenstate $1/\sqrt{2}$ $(|6, 4\rangle - |4, 6\rangle)$. The observed avoided level crossings in our experiments allow us to determine the longitudinal anisotropy parameter $D = 1.28$ K and the isotropic exchange constant $J = 0.8$ K.

Fig. 5 shows the tunnel splittings Δ of the different level anticrossings within the ground state multiplet (at $\mu_0H_z \approx 0.45$ T, 0.9 T and 1.35 T) and the ones involving excited spin multiplets (at $\mu_0H_z \approx 1.2$ T and 1.65 T) as a function of the transverse magnetic field μ_0H_x. Note that the tunnel splittings of the two antisymmetric level anticrossings around $\mu_0H_z \approx 1.6$ T could not be studied separately as they are too close.

In order to determine the tunnel splittings the longitudinal magnetic field was swept over a level anticrossing with fixed sweep rate $dH_z/dt = 68$ mT s^{-1} and fixed transverse magnetic

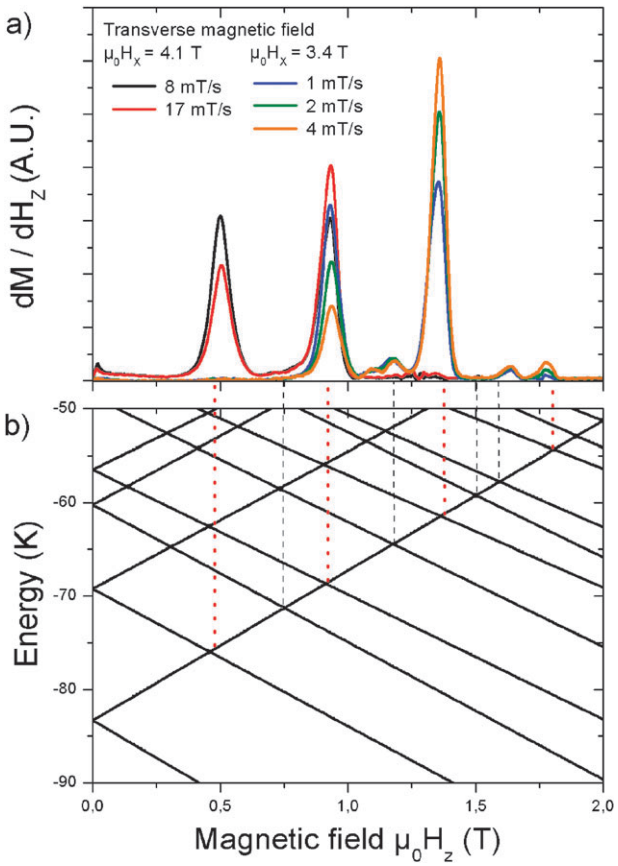

Fig. 4 (a) The derivative plot of some of the magnetization curves of Mn_6 of Fig. 3 shows various peaks due to tunnel transitions. In between the main tunnel transitions between states belonging to the ground state multiplet we observe a fine structure of additional tunnel transitions involving excited spin multiplets. (b) Zeeman diagram with tunnel transitions between symmetric spin states within the ground state multiplet (marked by red dotted lines) and tunnel transitions from the ground state multiplet to spin states belonging to excited spin multiplets (marked by black dashed lines).

field μ_0H_x and the probability of tunnelling from one state to the other was measured by means of magnetization decrease of the saturated sample.

The tunnel probability $P_{m,m'}$ between two spin states m and m' is given by the Landau–Zener formula

$$P_{m,m'} = 1 - \exp\left(-\frac{\pi\Delta_{m,m'}^2}{2\hbar g\mu_B|m-m'|dH_z/dt}\right) \qquad (3)$$

that allows us to calculate the tunnel splitting of the avoided level crossing $\Delta_{m,m'}$ when $P_{m,m'} \ll 1$.[5,19–22] Note that $P_{m,m'} \ll 1$ is not fulfilled for very high transverse magnetic fields and therefore the experimentally obtained tunnel splittings are only estimates of a lower boundary of $\Delta_{m,m'}$.[16] The experimentally obtained tunnel splittings lie in the range of 10^{-7} K for all the observed transitions and they rapidly increase when applying a transverse magnetic field $\mu_0H_x > 3$ T.

When calculating the tunnel splittings of the anticrossings between symmetric states they are mainly determined by the symmetric spin operators like the second and fourth order anisotropy terms or the Heisenberg exchange interaction.

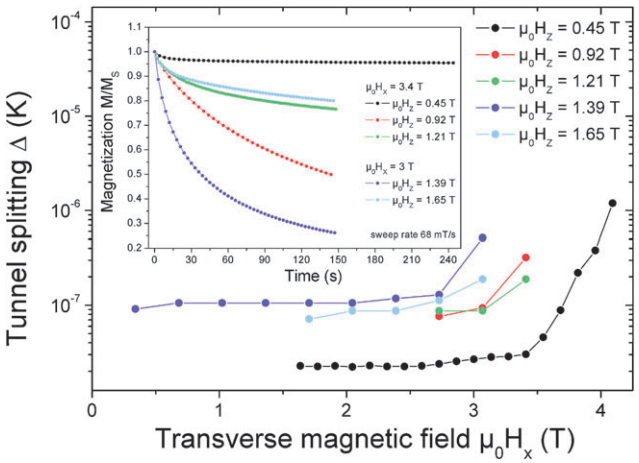

Fig. 5 Tunnel splittings Δ of Mn_6 as a function of the transverse magnetic field for different level anticrossings. The longitudinal magnetic field $\mu_0 H_z$ was swept over an avoided level crossing at a constant sweep rate $dH_z/dt = 68$ mT s^{-1} and with fixed transverse magnetic field. The tunnel splittings were obtained by applying the Landau–Zener technique.[6,24–26] The inset shows the time dependence of the magnetization of the saturated sample when sweeping several times over the level anticrossings.

However the splitting between a symmetric and an antisymmetric spin state is given by the matrix element involving antisymmetric spin operators, *i.e.* in the framework of our model the antisymmetric DM interaction. When analyzing the tunnel splitting between a symmetric and an antisymmetric spin state we can get an estimate of the DM interaction vector $\boldsymbol{D}_{12}$.

Further on, the magnitude of the tunnel splitting between symmetric spin states can be used to fix the parameters D, J and possible fourth order parameters. Numerical simulations of the tunnel splittings by exact diagonalization of the above defined Hamiltonian show that the isotropic exchange and weak higher order transverse anisotropy terms together with a transverse magnetic field comparable to the one used in the experiments give rise to tunnel splittings between states of the ground state multiplet of the order of 10^{-7} K.

The magnitude of the tunnel splittings is well reproduced when introducing a weak fourth order spin operator term as proposed by Carretta *et al.*[14] The strong increase in the tunnel splitting $\Delta_{m,m'}$ for large transverse magnetic fields is also well reproduced in the framework of this model. The large tunnel splittings between symmetric and antisymmetric spin states cannot be reproduced by any symmetric spin operator like second and fourth order crystal field anisotropy terms or the Heisenberg exchange interaction.

However, the antisymmetric DM exchange interaction can provide a quite large coupling between the symmetric and antisymmetric spin states. Numerical simulations show that a vector of the DM interaction $\boldsymbol{D}_{12}$ with components $D_x = D_y = D_z = 10$ mK gives rise to tunnel splittings of the order of the experimentally observed ones. In particular, the calculated tunnel splitting at $\mu_0 H_z \approx 0.75$ T turns out to be at least one order of magnitude smaller than the one at $\mu_0 H_z \approx 1.2$ T. This is consistent with our experiments, as we did not observe any clear and pronounced step in the magnetization curves at $\mu_0 H_z \approx 0.75$ T. The corresponding tunnel splitting is theoretically—with the parameters given above and transverse magnetic fields below 4 T—smaller than 10^{-8} K and therefore too small to be measured with our experimental technique.

Tunnel transitions at high longitudinal magnetic field

In addition to the tunnel transitions at low longitudinal magnetic field with high transverse magnetic field we study in this paragraph the tunnel transitions at low temperatures with no transverse magnetic fields. In this case the tunnel splittings at low longitudinal magnetic fields are very weak and will not be observed in our experiments. However the reversing of the magnetization of the molecule occurs at higher longitudinal magnetic fields where the probability for tunnel transitions between different spin states is high enough to be observed experimentally even without the presence of transverse magnetic fields.

Fig. 6 shows the magnetization measurements as a function of the longitudinal magnetic field for different temperatures in the range between 100 mK and 960 mK. The sample was first saturated in a large negative magnetic field and then the external magnetic field was ramped at constant magnetic field sweep rate $v = 1$ mT s^{-1} to positive field with no transverse magnetic fields applied.

The magnetization of the sample starts to relax at quite high magnetic fields of about 4 T. Typically the magnetization of the molecules is completely reversed in a longitudinal magnetic field above 5.2 T. We can distinguish in our experiments between a multitude of different tunnel transitions as a function of the temperature. Some tunnel transitions appear even at the very low temperature of 100 mK and others are thermally activated and start to appear at temperatures above 600 mK.

In order to better observe the positions of the tunnel transitions, we plotted the derivatives of the magnetization curves dM/dH as a function of the longitudinal magnetic field in Fig. 7. In this representation we can clearly distinguish

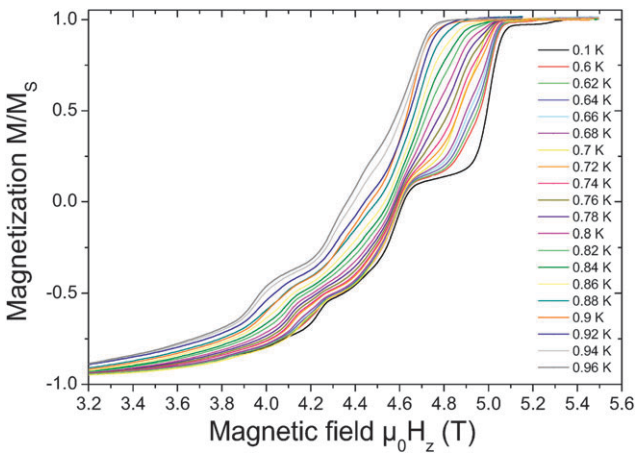

Fig. 6 Magnetization measurements of Mn_6 as a function of the longitudinal magnetic field for different temperatures in the range between 100 mK and 960 mK. The sample was first saturated in a large negative magnetic field and then the external magnetic field was ramped at constant sweep rate $dH_z/dt = 1$ mT s^{-1} to positive field with no transverse magnetic fields applied.

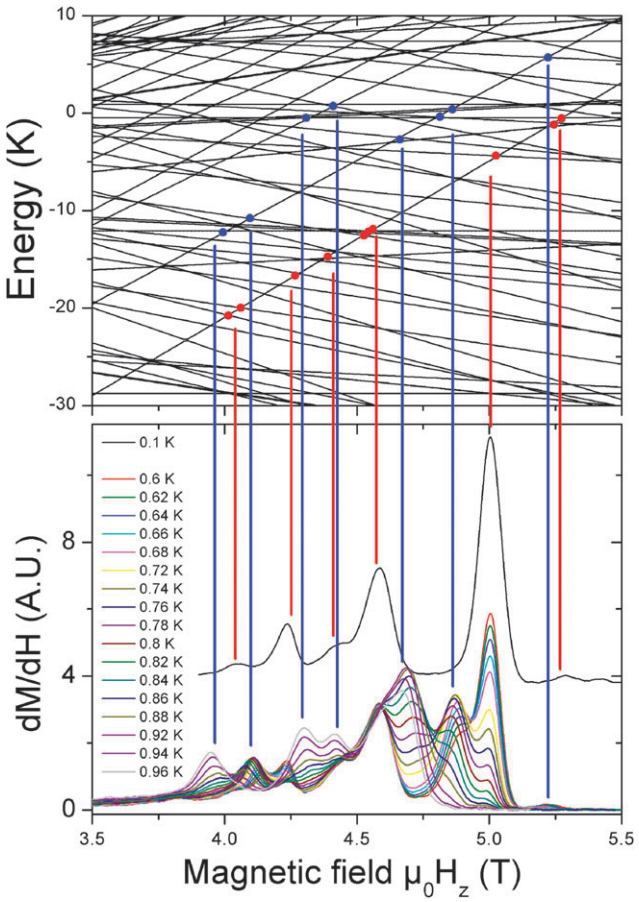

Fig. 7 Zeeman diagram of the dimeric molecule Mn_6 using the Hamiltonian parameters $D = 1.28$ K, $J = 0.8$ K, $g = 1.99$ and derivation dM/dH_z of the magnetization curves of Fig. 6 as a function of the longitudinal magnetic field. The local maxima of the experimental curves as a function of the temperature reveal a very rich structure and allow distinguishing between tunnel transitions in the ground state and thermally excited tunnel transitions. Note that the low temperature measurement at 100 mK is voluntarily shifted upwards to allow better discrimination of ground state tunnelling and thermal excited tunnel transitions.

between thermally excited tunnel transitions and tunnel processes of the fundamental spin states.

We can in addition numerically simulate the energy of the numerous spin states in the dimeric model of the molecule and we observe numerous crossings of spin states in the Zeeman diagram. As the tunnel splittings between a symmetric and an antisymmetric spin eigenstate should be very small (as the antisymmetric DM interaction is very weak and as we work in the absence of any transverse magnetic fields) we do not consider these antisymmetric tunnel transitions in the discussion of our experimental results.

As shown in Fig. 7 in the case of the tunnel transitions at very low temperature the tunnelling process involves the fundamental spin eigenstate $|-6, -6\rangle$ and another symmetric spin eigenstate that can be described in a good approximation by $(m_1,m_2) \equiv 1/\sqrt{2}\ (|m_1,m_2\rangle + |m_2,m_1\rangle)$. In fact most of the spin eigenstates in the Zeeman diagram are largely dominated by the symmetric superposition of the two spin states $|m_1,m_2\rangle$ and $|m_2,m_1\rangle$. Additional contributions from other spin states are negligibly small (their contribution to the wavefunction is very often a hundred times smaller than those of the leading terms) and will not be considered for clarity reasons.

We observe in Fig. 7 in the low temperature measurements at 100 mK six very pronounced tunnel transitions that appear at longitudinal magnetic fields of $\mu_0 H_z = 4.04$ T, 4.23 T, 4.42 T, 4.59 T, 5.00 T and 5.28 T. These experimentally observed tunnel transitions can be confirmed by numerical simulations using eqn (1) and (2). We find in our simulations at those six magnetic field positions level crossings of symmetric spin eigenstates that involve the fundamental spin state $|-6, -6\rangle$ and another symmetric spin eigenstate. The results of the numerical simulations for the low temperature tunnel transitions and the corresponding spin eigenstates are summarized in Table 1.

In fact in the Zeeman diagram of Fig. 7 we observe a lot more level crossings than in our experiments. Many of the level crossings involve the fundamental spin eigenstate $|-6, -6\rangle$ and another antisymmetric spin eigenstate. These transitions between a symmetric spin state and an antisymmetric spin state are supposed to be very weak and therefore we do not observe all these potential tunnel transitions in our experiments. Only the transitions between two symmetric spin states are large enough to contribute sufficiently in our experiments to the magnetization reversal.

In order to explain theoretically the thermally excited tunnel transitions we looked for spin level crossings in the Zeeman diagram of Fig. 7 which involves two excited and symmetric spin eigenstates. We found in our numerical simulations various level crossings that involve the excited spin states $|S = 12, M = -11\rangle = 1/\sqrt{2}(|-6, -5\rangle + |-5, -6\rangle) \equiv (-5;-6)$ and $|S = 12, m = -10\rangle \equiv (-5;-5)$.

The results of the thermal excited tunnel transitions of our experiments in the temperature range between 600 mK and 960 mK and the corresponding numerical simulations are summarized in Table 2. The level crossings of symmetric and excited spin states appear approximately at the experimentally observed magnetic field positions. The experimentally observed tunnel transition at $\mu_0 H_z = 3.95$ T for example can be explained by the level crossing of the excited spin state $|S = 12, m = -11\rangle \equiv (-5;-6)$ and the symmetric spin state $|S, m\rangle \approx 1/\sqrt{2}(|-5, 5\rangle + |5, -5\rangle) \equiv (-5;5)$. The other thermally excited tunnel transitions can also be explained by

Table 1 Experimental tunnel transitions of Mn_6 at high longitudinal magnetic field. The experimentally observed tunnel transitions at 100 mK can be assigned to two well-defined spin states in the dimeric model of the molecule. The numerical simulations involve the Hamiltonian parameters $D = 1.28$ K, $J = 0.8$ K, $g = 1.99$

Experiment/T	Theory/T	Initial state (m_1,m_2)	Final state (m_1,m_2)
4.04	4.02	(−6;−6)	(5;0)
4.04	4.06	(−6;−6)	(3;0)
4.23	4.27	(−6;−6)	(5;−1)
4.42	4.38	(−6;−6)	(5;−6)
4.59	4.54	(−6;−6)	(5;−2)
4.59	4.54	(−6;−6)	(5;−4)
4.59	4.56	(−6;−6)	(5;−5)
5.00	5.03	(−6;−6)	(1; 0)
5.28	5.23	(−6;−6)	(4;−6)
5.28	5.28	(−6;−6)	(3;−3)

Table 2 Experimental tunnel transitions at high longitudinal magnetic field for the observed thermally activated tunnel transitions. They can be assigned to two well-defined spin states in the dimeric model of the molecule. The numerical simulations involve the Hamiltonian parameters $D = 1.28$ K, $J = 0.8$ K, $g = 1.99$

Experiment/T	Theory/T	Initial state (m_1,m_2)	Final state (m_1,m_2)
3.95	3.99	(−5;−6)	(5;−5)
4.09	4.09	(−5;−6)	(5;−2)
4.30	4.32	(−5;−5)	(−3;3)
4.30	4.32	(−5;−5)	(4;−5)
4.42	4.42	(−5;−5)	(4; 0)
4.68	4.65	(−5;−6)	(4;−6)
4.85	4.80	(−5;−6)	(3;−3)
4.85	4.85	(−5;−6)	(4;−5)
5.23	5.22	(−5;−6)	(5;−4)

different level crossings of symmetric spin states as depicted in Fig. 7 and Table 2.

Finally we remark that in the framework of a dimeric molecule where the spin eigenstates contributing to one tunnel transition can be described by one dominant spin state (m_1,m_2) these tunnel transitions can be understood as a spin–spin cross-relaxation in the molecule.[23] In fact when the molecule tunnels between two spin states, the two halves of the molecule change simultaneously their spin state in order to minimize their interaction energy with each other and with the external magnetic field.

Conclusions

We have presented magnetization measurements of the SMM Mn_6 revealing various tunnel transitions. At low longitudinal magnetic fields with the presence of high transverse magnetic fields we observed several tunnel transitions, which are forbidden in the framework of a giant spin approximation. We propose to describe the Mn_6 SMM as a molecular dimer of two coupled spins $S = 6$. The introduction of an antisymmetric exchange interaction leads to the superposition of spin states with different spin length. This superposition of spin states belonging to different multiplets leads to additional tunnel transitions which are observed in our experiments.

In addition we presented magnetization measurements at high longitudinal magnetic fields with no transverse magnetic fields that reveal a very rich structure of tunnel transitions. In the framework of the dimeric molecular structure we were able to explain the numerous fundamental and thermally excited tunnel transitions.

Therefore we found strong evidence that this molecular dimer description of this SMM is well justified, especially at low temperatures and small longitudinal magnetic fields. It is obvious that the presented simple dimer description is only valid for the description of the lowest spin multiplets and possible effects of higher excited spin multiplets are probably not well described by this simple model. Nevertheless, this multi-spin description goes far beyond the standard giant spin approximation and is capable of explaining the experimentally observed tunnel transitions. This dimeric model of the molecule is confirmed by numerical calculations of the positions and the magnitude of the tunnel splittings which are consistent with our experimental results.

Acknowledgements

This work is partially financed by EC-RTN-QUEMOLNA Contract No. MRTN-CT-2003-504880, MAGMANet, ERC and ANR MolNanoSpin. We thank E. Eyraud and D. Lepoittevin for technical support.

References

1 G. Christou, D. Gatteschi, D. N. Hendrickson and R. Sessoli, *MRS Bull.*, 2000, **25**, 66.
2 D. A. Garanin, X. M. Hidalgo and E. M. Chudnovsky, *Phys. Rev. B: Condens. Matter Mater. Phys.*, 1998, **57**, 13639.
3 J. R. Friedman, M. P. Sarachik, J. Tejada and R. Ziolo, *Phys. Rev. Lett.*, 1996, **76**, 3830.
4 L. Thomas, F. Lionti, R. Ballou, D. Gatteschi, R. Sessoli and B. Barbara, *Nature*, 1996, **383**, 145.
5 A. Garg, *Europhys. Lett.*, 1993, **22**, 205.
6 W. Wernsdorfer and R. Sessoli, *Science*, 1999, **284**, 133.
7 M. N. Leuenberger and D. Loss, *Nature*, 2001, **410**, 789.
8 F. Troiani, A. Ghirri, M. Affronte, S. Carretta, P. Santini, G. Amoretti, S. Piligkos, G. A. Timco and R. E. P. Winpenny, *Phys. Rev. Lett.*, 2005, **94**, 207208.
9 A. Ardavan, O. Rival, J. J. L. Morton, S. J. Blundell, A. M. Tyryshkin, G. A. Timco and R. E. P. Winpenny, *Phys. Rev. Lett.*, 2007, **98**, 057201.
10 L. Bogani and W. Wernsdorfer, *Nat. Mater.*, 2008, **7**, 179.
11 A.-L. Barra, P. Debrunner, D. Gatteschi, Ch. E. Schulz and R. Sessoli, *Europhys. Lett.*, 1996, **35**, 133.
12 K. Petukhov, S. Hill, N. E. Chakov, K. A. Abboud and G. Christou, *Phys. Rev. B: Condens. Matter Mater. Phys.*, 2004, **70**, 054426.
13 S. Carretta, P. Santini, G. Amoretti, T. Guidi, J. R. D. Copley, Y. Qiu, R. Caciuffo, G. Timco and R. E. P. Winpenny, *Phys. Rev. Lett.*, 2007, **98**, 167401.
14 S. Carretta, T. Guidi, P. Santini, G. Amoretti, O. Pieper, B. Lake, J. van Slageren, F. El Hallak, W. Wernsdorfer, H. Mutka, M. Russina, C. J. Milios and E. K. Brechin, *Phys. Rev. Lett.*, 2008, **100**, 157203.
15 C. M. Ramsey, E. del Barco, S. Hill, S. J. Shah, C. C. Beedle and D. N. Hendrickson, *Nat. Phys.*, 2008, **4**, 277.
16 W. Wernsdorfer, arXiv:0804.1246v3.
17 S. Bahr, C. J. Milios, L. F. Jones, E. K. Brechin, V. Mosser and W. Wernsdorfer, *Phys. Rev. B: Condens. Matter Mater. Phys.*, 2008, **78**, 132401.
18 W. Wernsdorfer, T. C. Stamatatos and G. Christou, *Phys. Rev. Lett.*, 2008, **101**, 237204.
19 C. J. Milios, A. Vinslava, W. Wernsdorfer, S. Moggach, S. Parsons, S. P. Perlepes, G. Christou and E. K. Brechin, *J. Am. Chem. Soc.*, 2007, **129**, 2754.
20 K. Petukhov, S. Bahr, W. Wernsdorfer, A.-L. Barra and V. Mosser, *Phys. Rev. B: Condens. Matter Mater. Phys.*, 2007, **75**, 064408.
21 S. Bahr, K. Petukhov, V. Mosser and W. Wernsdorfer, *Phys. Rev. Lett.*, 2007, **99**, 147205.
22 W. Wernsdorfer, N. E. Chakov and G. Christou, *Phys. Rev. B: Condens. Matter Mater. Phys.*, 2004, **70**, 132413.
23 W. Wernsdorfer, S. Bhaduri, R. Tiron, D. N. Hendrickson and G. Christou, *Phys. Rev. Lett.*, 2002, **89**, 197201.
24 W. Wernsdorfer, R. Sessoli, A. Caneschi, D. Gatteschi, A. Cornia and D. Mailly, *J. Appl. Phys.*, 2000, **87**, 5481.
25 W. Wernsdorfer, M. Murugesu and G. Christou, *Phys. Rev. Lett.*, 2006, **96**, 057208.
26 W. Wernsdorfer, R. Sessoli, A. Caneschi, D. Gatteschi and A. Cornia, *Europhys. Lett.*, 2000, **50**, 552.

